Measuring the Spectral Form Factor in Many-Body Chaotic and Localized Phases of Quantum Processors

Hang Dong,[1,*] Pengfei Zhang,[1,*] Ceren B. Dağ,[2,3] Yu Gao,[1] Ning Wang,[1] Jinfeng Deng,[1] Xu Zhang,[1] Jiachen Chen,[1] Shibo Xu,[1] Ke Wang,[1] Yaozu Wu,[1] Chuanyu Zhang,[1] Feitong Jin,[1] Xuhao Zhu,[1] Aosai Zhang,[1] Yiren Zou,[1] Ziqi Tan,[1] Zhengyi Cui,[1] Zitian Zhu,[1] Fanhao Shen,[1] Tingting Li,[1] Jiarun Zhong,[1] Zehang Bao,[1] Hekang Li,[1] Zhen Wang,[1] Qiujiang Guo,[1] Chao Song,[1] Fangli Liu,[4] Amos Chan,[5,†] Lei Ying,[1,‡] and H. Wang[1,§]

[1]*School of Physics, ZJU-Hangzhou Global Scientific and Technological Innovation Center, and Zhejiang Key Laboratory of Micro-nano Quantum Chips and Quantum Control, Zhejiang University, Hangzhou, China*

[2]*ITAMP, Harvard-Smithsonian Center for Astrophysics, Cambridge, Massachusetts 02138, USA*

[3]*Department of Physics, Harvard University, Cambridge, Massachusetts 02138, USA*

[4]*QuEra Computing Inc., 1284 Soldiers Field Road, Boston, Massachusetts 02135, USA*

[5]*Department of Physics, Lancaster University, Lancaster LA1 4YB, United Kingdom*

(Received 7 May 2024; accepted 25 November 2024; published 2 January 2025)

The spectral form factor (SFF) captures universal spectral fluctuations as signatures of quantum chaos, and has been instrumental in advancing multiple frontiers of physics including the studies of black holes and quantum many-body systems. The measurement of the SFF in many-body systems is however challenging due to the difficulty in resolving level spacings that become exponentially small with increasing system size. Here, we utilize the random measurement toolbox to perform a direct experimental measurement of the SFF, and hence probe the presence or absence of chaos in quantum many-body systems on superconducting quantum processors. For a Floquet chaotic system, we observe signatures of both short- and long-range spectral correlations in the SFF given by the ramp-plateau behavior. Furthermore, for a Hamiltonian system we utilize the SFF to distinguish a quantum many-body chaotic phase and the prethermal many-body localization. We observe the dip-ramp-plateau behavior of random matrix theory in the chaotic phase and contrast the scaling of the plateau time in system size between the many-body chaotic and localized phases. Finally, we probe the eigenstate statistics by measuring a generalization of the SFF, known as the partial SFF, and observe distinct behaviors in the purity of the reduced density matrices in these two phases. This work unveils a new experimental way of extracting the universal signatures of many-body quantum chaos in quantum devices by probing short- and long-range correlations in the energy spectrum and eigenstates.

DOI: 10.1103/PhysRevLett.134.010402

Spectral statistics is a powerful tool for analyzing quantum systems, as it captures the correlations between eigenenergies and reveals the universal features inherent to such systems. It has served as a longstanding diagnostic of quantum chaos as described by the Bohigas-Giannoni-Schmidt conjecture [1]: A quantum system can be considered chaotic if its spectral statistics resemble those found in random matrix theory (RMT) [2] at sufficiently small energy scales. Historically, spectral statistics and RMT have been applicable in a wide range of fields, including complex atomic nuclei [3,4], number theory [5,6], quantum chaos [1,7], and quantum transport in mesoscopic systems [8,9]. Experimentally, only the nearest-neighbor level spacing statistics have been probed by extracting the energy levels from the Fourier transform of a time-dependent correlation function [10] or from spectroscopy measurements [11–14], which captures the short-range energy level correlations. Such protocols are challenging for many-body systems due to the difficulty in resolving level spacings that become exponentially small with increasing system size. Beyond spectral correlations, another important diagnostic of quantum chaos and thermalization, concerning eigenstate correlations, is the eigenstate thermalization hypothesis (ETH) [15–17]. The ETH postulates that in sufficiently narrow energy windows, the matrix elements of few-body operators in the energy eigenstate behave in a typical way as captured by the RMT, thereby providing an explanation of thermalization in isolated quantum systems through the understanding of correlations among eigenstates. Spectral statistics and eigenstate correlations serve as two defining diagnoses for the presence (or absence) of quantum chaos and thermalization, and therefore their experimental

*These authors contributed equally to this work.
†Contact author: amos.chan@lancaster.ac.uk
‡Contact author: leiying@zju.edu.cn
§Contact author: hhwang@zju.edu.cn

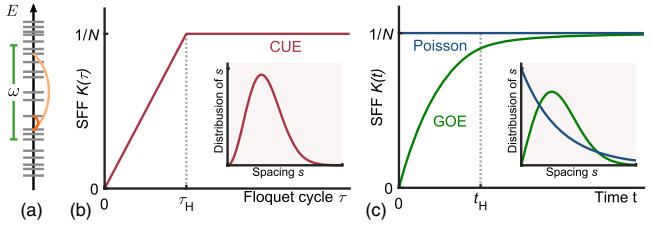

FIG. 1. Schematics of the SFF. (a) Spectral correlations concern the likelihood of finding two levels with a certain distance ω, and it can be probed in the time domain by its Fourier transform known as the SFF. (b) Floquet quantum chaotic systems without time-reversal symmetry [c.f. Fig. 2] display universal SFF behavior that can be captured by random matrix ensembles known as the circular unitary ensemble (CUE). The CUE behavior displays a ramp followed by a plateau after the Heisenberg time t_{H}, and the behavior around t_{H} is also often probed with reference to the Wigner-Dyson distribution in the inset, which is the nearest-neighbor energy spacing distribution found in the RMT. (c) Quantum chaotic systems with time-reversal symmetry [c.f. Fig. 3] display universal SFF behavior of the Gaussian orthogonal ensemble (GOE, in green), while the SFF of localized systems can be captured by Poisson distribution (blue). The corresponding spacing distributions are given in the inset.

measurements are of immense interest in the study of out-of-equilibrium dynamics in quantum many-body systems.

The spectral form factor (SFF) is the Fourier transform of the two-level correlation function—the probability of finding two eigenenergies with a certain distance in the energy spectrum [Fig. 1(a)]. The SFF is arguably the simplest analytically tractable quantity to capture not only the short-range, but also the long-range universal spectral fluctuations of quantum systems, and consequently, it has been instrumental in multiple frontiers of physics, such as the semiclassical approach to quantum chaos [7,18–20], black holes [21–24], many-body quantum chaos [25–28], and transition to prethermal many-body localization (MBL) [29–32] and more [33–44]. Formally, the SFF can be defined as

$$K(t) = \frac{1}{N^2}\overline{\left|\mathrm{Tr}\hat{U}(t)\right|^2} = \frac{1}{N^2}\overline{\sum_{a,b} e^{i(E_a - E_b)t}}, \tag{1}$$

where $\hat{U}(t)$ is the time evolution operator of the system of interest, defined through either a time-independent Hamiltonian via $\hat{U}(t) \coloneqq \exp\left(-i\hat{H}t\right)$, or a time-periodic Hamiltonian via $\hat{U}(t = \tau T) = \hat{U}^{\tau}$ with Floquet operator $\hat{U} \coloneqq \hat{\mathcal{T}} \exp\left(-i\int_0^T \mathrm{d}t' \hat{H}(t')\right)$, where $\hat{\mathcal{T}}, T$, and τ are the time-ordering operator, the Floquet period, and the number of Floquet cycles, respectively. $\{E_a\}$ are the eigenenergies or quasienergies of $\hat{H}$ and $\hat{U}$, respectively. N is the Hilbert space dimension, and $\overline{(\ldots)}$ denotes the ensemble average over statistically similar systems. We adopt the convention where $K(t)$ is normalized such that $K(0) = 1$. For quantum many-body systems, a generalization of the SFF called the partial spectral form factor (pSFF) [45–47] has been introduced by partitioning the many-body system, and was utilized to probe eigenstate correlations in addition to spectral statistics. Benefiting from the development of quantum simulators [48,49], and protocols that utilize randomized sampling and repeated measurements [45,50], we measure the SFF and pSFF in superconducting quantum simulators to diagnose signatures of quantum chaos and localization in periodically driven and time-independent quantum many-body systems.

Our superconducting many-body quantum simulators have one-dimensional arrays of individually controllable qubits with tunable nearest-neighbor couplings [51]. Specifically, we simulate a one-dimensional XY model, $\hat{H}_{XY} = J\sum_m^{L-1}(\hat{\sigma}_m^+\hat{\sigma}_{m+1}^- + \hat{\sigma}_m^-\hat{\sigma}_{m+1}^+)$, along with time-varying potential on each qubit of the form, $h_m^{\alpha}(t)\hat{\sigma}_m^{\alpha}$. Here, J and L denote the strength of tunable nearest-neighbor coupling, and the number of qubits in the chain, respectively. $\hat{\sigma}_m^{\alpha}$ denotes a Pauli matrix acting on the mth qubit with $\alpha = x, y, z$. The driving $h_m^{\alpha}(t)$ of the mth qubit along the α axis can be individually and dynamically tuned, allowing us to simulate both many-body Floquet and time-independent Hamiltonian systems.

We first program one of the simulators to implement a Floquet system whose model can be constructed so that all global symmetries and conserved quantities, including energy, are removed. Our Floquet model with L qubits is defined by [Fig. 2(a)]

$$\hat{H}(t) = \begin{cases} \hat{H}^x, & 0 \le t/T < 1/3, \\ \hat{H}^z, & 1/3 \le t/T < 2/3, \\ \hat{H}^y, & 2/3 \le t/T < 1, \end{cases}$$
$$\hat{H}^{\alpha} = \hat{H}_{XY} + \sum_{m=1}^{L} h_m^{\alpha}\hat{\sigma}_m^{\alpha}, \tag{2}$$

where the coupling strength $J/2\pi$ in $\hat{H}_{XY}$ is tuned to be -5 MHz. The local potentials h_m^{α} are randomly and independently sampled from a uniform distribution over a range of $[-W, W]$ with $W/2\pi = 5$ MHz, which corresponds to $[-1, 1]J$. The periods T are chosen to be 150 ns for $L = 2, 3$, and 90 ns for $L = 4, 5$ [51]. The integrability in this model is broken due to the driving. For quantum chaotic systems with Hilbert space size N and without symmetries, the behavior of the SFF can be modeled by the circular (or Gaussian) unitary ensemble (CUE) in the RMT of N-by-N unitary matrices. Correspondingly the SFF $K(\tau)$ at Floquet cycle τ displays a characteristic feature known as the "ramp-plateau behavior" [see Eq. (A1)] [2], as depicted in Fig. 1(b). Here $\tau_{\mathrm{H}} = N$ is the analog of the Heisenberg time in Floquet systems, which is a dimensionless quantity proportional to the inverse of the mean quasienergy level spacing. The transition between the ramp and plateau at the

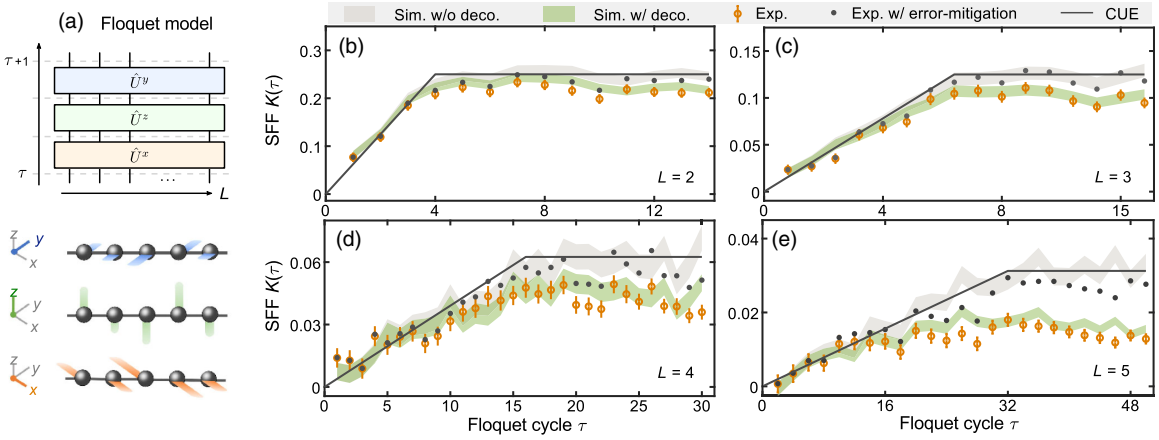

FIG. 2. Experimental measurement of the SFF for a Floquet quantum many-body system, Eq. (2), in the chaotic phase. (a) Illustration of the Floquet system, with time-dependent driving along the x, z, y axes within a single Floquet cycle. (b)–(e) SFF of the Floquet system against the number of Floquet cycles with system sizes up to $L = 5$ for 400 to 1000 realizations. The experimental data, error-mitigated data, simulations, and RMT prediction are plotted in circles, black dots, shaded areas, and lines respectively. The error bars represent the standard error of mean.

Heisenberg time τ_{H} reflects the same physics captured by level repulsion, see inset in Fig. 1(c).

Figures 2(b)–2(e) show the experimental data on the SFF of the Floquet model for $L = 2$–5. After taking decoherence into account (see below), we find a good qualitative agreement between the experimental data and the numerical simulation. The ramp-plateau RMT behavior is apparent, especially for the smaller system sizes in early time when the decoherence effects are not prominent. We observe that the plateau time, τ_{p}, defined to be the time when the plateau begins, approximately coincides with the Heisenberg time $\tau_{\mathrm{H}} = N = 2^L$. The observation of the ramp-plateau behavior is compelling evidence that this system is in the chaotic phase. Decoherence in the quantum processor lowers the value of $K(\tau)$, leading to deviations between the experimental measurement of $K(\tau)$ and the theoretical prediction $K(\tau)$ in the absence of decoherence.

To understand the deviations, we simulate the experimental protocol including the decoherence parameters [51], and find that the numerics are in qualitative agreement with the experimental data (Fig. 2). Since τ_{H} scales exponentially with the system size, the observation of the ramp-plateau behavior for larger systems at late time is more prone to decoherence. See the Appendix for the details on error mitigation. Next, we program the simulator to implement a one-dimensional time-independent many-body Hamiltonian defined by

$$\hat{H} = \hat{H}_{XY} + h^x \sum_m^L \hat{\sigma}_m^x + \sum_m^L h_m^z \hat{\sigma}_m^z, \tag{3}$$

where the coupling strength $J/2\pi$ in $\hat{H}_{XY}$ and transverse field $h^x/2\pi$ are configured at -5 MHz and 2 MHz (i.e., $h^x/J = -0.4$), respectively. The local potentials h_m^z are randomly and independently sampled from a uniform distribution within the range $[-W, W]$. The value of W determines the dynamical regime of the system—whether it exhibits the characteristics of quantum chaotic or prethermal MBL systems. Although the stability of the MBL phase in the thermodynamic limit is currently under debate [31,52], our experimental system is a finite-size system, and MBL can exist as a metastable state.

In the presence of time-reversal symmetry with the time-reversal symmetry operator squaring to identity, quantum chaotic systems display RMT spectral statistics as described by the Gaussian (or circular) orthogonal ensemble (GOE). The connected SFF [53] of the GOE also exhibits a ramp-plateau behavior, however, with a smoothed kink as in Eq. (A2). Whereas for MBL, spectral statistics can be modeled by Poisson distribution with SFF quickly approaching N^{-1} [32,54] [Fig. 1(c)].

The measurement results and numerical simulations of the SFF for the time-independent Hamiltonian both in chaotic and prethermal MBL phases are shown in Figs. 3(c)–3(f) for system sizes up to $L = 5$. For both cases, for sufficiently large time, the SFF will reach the plateau at the plateau time t_{p}. For $W/2\pi = 5$ MHz ($W/J = 1$), the SFF displays an initial dip, a ramp, and a plateau with t_{p} scaling exponentially in the system size. The experimental data are in qualitative agreement with the numerical simulation and theoretical prediction from the RMT, suggesting that the system is in the chaotic phase and that t_{p} can be identified as t_{H} of the system. For $W/2\pi =$ 50 MHz ($W/J = 10$), the SFF dips and then plateaus relatively quickly, at times much earlier than the case of $W = J$. Crucially, unlike the chaotic case, t_{p} does not increase exponentially with system size [Fig. 3(b)], which is consistent with the expectation of a prethermal MBL phase. These two cases are also numerically confirmed by

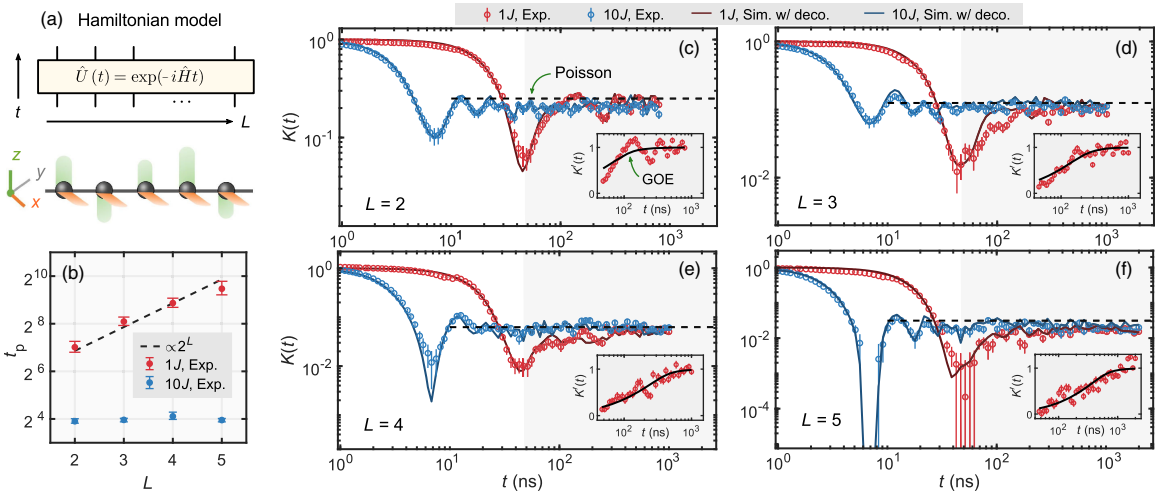

FIG. 3. Experimental measurement of the SFF for a Hamiltonian system, Eq. (3), in the chaotic and prethermal MBL phases. (a) Illustration of the Hamiltonian system, which is simulated in the chaotic phase with $W = J$ and prethermal MBL phase with $W = 10J$ for 400 to 1000 realizations up to the system size $L = 5$. (b) The plateau time t_p of the SFF increases exponentially in L in the chaotic phase (red), but not in the prethermal MBL phase (blue). (c)–(f) SFF $K(t)$ of the Hamiltonian model in the chaotic phase (red) and the prethermal MBL phase (blue) for up to $L = 5$. The experimental data, simulations, and Poissonian statistics are plotted in circles, lines, and dashed lines, respectively. For each inset, we numerically fit the error-mitigated and normalized SFF data $K'(t)$ with the GOE RMT behavior, for the domain in the shaded region of the main panel starting from $t = 48$ ns when the SFF has reached its lowest value. See Supplemental Material for details of the determination of t_p, the fitting and error mitigation procedures. The error bars represent the standard error of mean.

calculating the $\langle r \rangle$ parameter originating from the nearest-neighbor level spacing statistics [51]. For both cases, the theoretical predictions from the RMT and the Poissonian distribution [Fig. 1] are fitted after the initial dip in error-mitigated SFF data [see insets in Figs. 3(c)–3(f)], to avoid the early-time nonuniversal SFF behavior appearing due to the inhomogeneities in the density of states [51].

The pSFF is a generalization of the SFF in quantum many-body systems that probes the correlations of eigenstates, in addition to the correlations of eigenenergies. Because of this feature, the pSFF can detect the signatures of thermalization, (prethermal) localization, or other ergodicity-breaking mechanisms exhibited in eigenstate correlations. Specifically, for a subsystem A and its complement B, the pSFF is defined as [45–47] $K_A(t) \coloneqq (1/NN_A)\overline{\mathrm{Tr}_B\left[\left|\mathrm{Tr}_A \hat{U}(t)\right|^2\right]}$, where N_A denotes the Hilbert space dimension of subsystem A, and Tr_A is the partial trace of subsystem A. Experimentally, the pSFF can be accessed using the randomized measurement protocol identical to the one of the SFF [45], except that only the random measurements in the subsystem A are taken. In Figs. 4(a) and 4(d), we experimentally measure and numerically simulate the pSFF for the Floquet and Hamiltonian models in the chaotic phase, respectively. After accounting for the effect of decoherence, we observe the RMT ramp-plateau behavior in $K_A(t)$ with a qualitative agreement between experimental data and numerical simulations. We also observe a vertical shift in $K_A(t)$ that is dependent on subsystem size, see Figs. 4(c) and 4(g). These qualitative features are consistent with the pSFF behavior for chaotic quantum many-body systems at sufficiently large time, such that the systems exhibit RMT behavior as given by [45], $K_A^{\mathrm{RMT}}(t) \approx K(t) + 1/N_A^2$, for $N_A, N/N_A \gg 1$. In Fig. 4(e), we measure the pSFF for the Hamiltonian model in the prethermal MBL phase. In contrast to the chaotic phase (as in the case of SFF), we observe that the pSFF quickly reaches the plateau with a plateau time t_p that does not scale with the system size. As in the chaotic case, the pSFF for MBL displays a subsystem-size-dependent shift, but the shift in the MBL case is larger than the one in the chaotic phase due to differences in eigenstate correlations in the two cases, as reflected in the purity discussion below. For all cases, by analyzing the data after the removal of the vertical shift, we observe that the plateau time t_p of pSFF does not display dependency on the subsystem size L_A, and coincides with the t_p of SFF.

The purity of the reduced density matrix of a subsystem B, defined by $p_B \coloneqq \mathrm{Tr}_B[\rho_B^2]$, quantifies the entanglement between the subsystem and its complement, and is related to the second Renyi entropy via $S_2(\rho_B) \coloneqq -\log p_B$. The averaged purity can be expressed in terms of the pSFF $K_A(t)$ for t much larger than the Heisenberg time t_H as $P_B \equiv (1/N)\overline{p_B} = \lim_{t_H/t \to 0} K_A(t) N_A$. In practice, since experimental data are collected in finite time (with finite-depth circuits) and the decoherence is increasingly dominant at late times, we obtain an estimation of the purity, $\tilde{P}_B$, by measuring the pSFF (for all cases) at ηt_H with $\eta = 1.2$. In Figs. 4(b) and 4(f), we present the experimental results with numerical simulations for the Floquet and

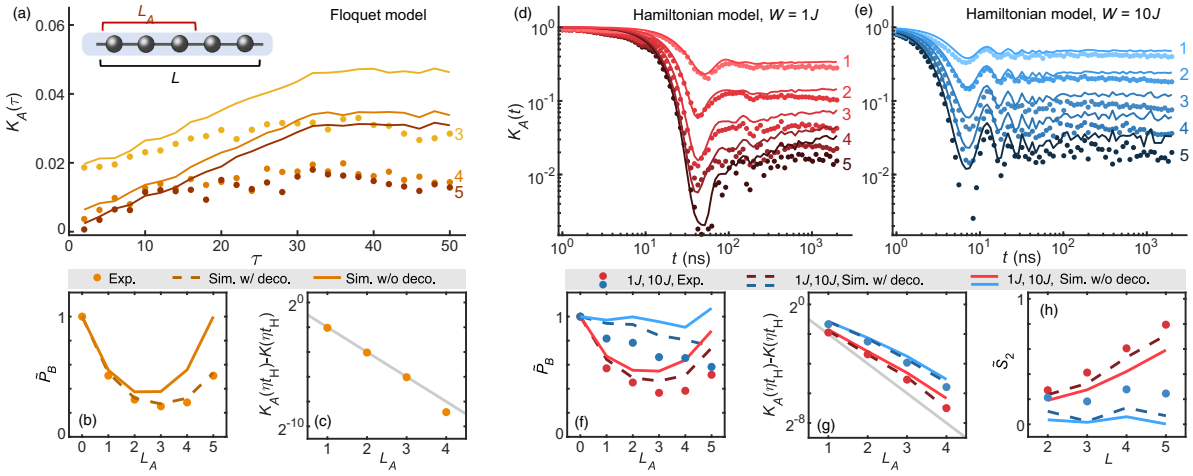

FIG. 4. Experimental measurement of the pSFF for the Floquet system, Eq. (2), and the Hamiltonian system, Eq. (3). The experimental measurement of the pSFF for the Floquet system in the chaotic phase (a), the Hamiltonian system in the chaotic phase (d), and the prethermal MBL phase (e). The system size for all cases is $L = 5$, and the integers toward the right of (a),(d),(e) denote the subsystem sizes $L_A \in [1, 5]$. We estimate the purity P_B of the subsystem B by measuring the long time behavior of pSFF, $\tilde{P}_B \equiv K_A(\eta t_{\mathrm{H}})N_A$ with $\eta = 1.2$ for (b) Floquet and (f) Hamiltonian systems. We measure the dependence of the shift on L_A in pSFF concerning the SFF by computing $K_A(\eta t_{\mathrm{H}}) - K(\eta t_{\mathrm{H}})$ for the (c) Floquet and (g) Hamiltonian systems. The gray lines are given by $N_A^{-2} = 2^{-2L_A}$. In (h), we plot the estimated half-system-size annealed average of the second Renyi entropy S_2 as a function of L by computing $\tilde{S}_2 \equiv -\log \tilde{P}_B$.

Hamiltonian models, respectively, which display decent agreement. We see a substantial difference in purity $\tilde{P}_B$ in the chaotic and localized cases, namely, that ρ_B is more mixed in the chaotic case compared to the localized case. Note that in the presence of decoherence, $\tilde{P}_B$ obtained under the current protocol [dots in Figs. 4(b) and 4(f)] is not symmetric under the exchange of L_A and $L - L_A$ [55] unlike the numerical simulations without decoherence channels (solid lines). With the accessible system sizes, we observe in Fig. 4(h) that the estimation of the half-system-size annealed average of second Renyi entropy, $\tilde{S}_2$, has a faster increase in the total system size in the chaotic case. These results demonstrate that, as anticipated, subsystems share more entanglement in chaotic quantum many-body systems than in prethermal MBL systems.

We have experimentally measured spectral form factors in quantum many-body superconducting processors, thereby demonstrating the effectiveness of such processors in probing the signatures of quantum chaos in spectral statistics and eigenstate correlations. For the first time to our knowledge, we observe the long-range spectral rigidity in both time-independent and periodically-driven quantum many-body systems by measuring the random matrix theory predicted ramp-plateau behavior in spectral form factors. Further, utilizing both the spectral form factor and partial spectral form factor as its generalization, we demonstrated the existence of a prethermal many-body localized regime in our time-independent setup and contrasted its eigenenergy and eigenstate correlations against those in the chaotic regime. The experimental measurement of form factors opens up exciting directions in charting the dynamical signatures of many-body quantum systems in the laboratory, such as the universal behavior of the spectral form factor in earlier times than the onset of random matrix theory [27,56–58], the emergence of random matrix theory universality in non-Hermitian systems [59], and the crossover between the chaotic and prethermal many-body localized regimes [31].

Acknowledgments—The device was fabricated at the Micro-Nano Fabrication Center of Zhejiang University. We are grateful to Minh-Thi Nguyen for helpful discussions. We acknowledge the support of the National Natural Science Foundation of China (Grants No. 92365301, No. 92065204, No. 12174342, No. 12274368, No. 12274367, No. 12375021, and No. U20A2076), the National Key Research and Development Program of China (Grants No. 2023YFB4502600 and No. 2022YFA1404203), and the Zhejiang Provincial Natural Science Foundation of China (Grant No. LR24A040002). A. C. acknowledges the support from the Royal Society (Grant No. RGS\R1\231444) and from the EPSRC Open Fellowship EP\X042812\1. C. B. D. acknowledges the support from the NSF through a grant for ITAMP (Grant No. 2116679) at Harvard University.

[1] O. Bohigas, M. J. Giannoni, and C. Schmit, Phys. Rev. Lett. **52**, 1 (1984).
[2] M. L. Mehta, *Random Matrices* (Elsevier, New York, 2004).
[3] C. E. Porter and R. G. Thomas, Phys. Rev. **104**, 483 (1956).

[4] T. A. Brody, J. Flores, J. B. French, P. A. Mello, A. Pandey, and S. S. M. Wong, Rev. Mod. Phys. **53**, 385 (1981).
[5] H. L. Montgomery, in *Proceedings of Symposia in Pure Mathematics* (1973), Vol. 24, pp. 181–193.
[6] J. P. Keating and N. C. Snaith, Commun. Math. Phys. **214**, 57 (2000).
[7] M. V. Berry, Proc. R. Soc. A **400**, 229 (1985).
[8] Y. Imry, Europhys. Lett. **1**, 249 (1986).
[9] B. L. Altshuler and B. I. Shklovskii, Sov. J. Exp. Theor. Phys. **91**, 220 (1986) [, Sov. J. Exp. Theor. Phys. **64**, 127 (1986)].
[10] P. Roushan *et al.*, Science **358**, 1175 (2017).
[11] R. U. Haq, A. Pandey, and O. Bohigas, Phys. Rev. Lett. **48**, 1086 (1982).
[12] A. Frisch, M. Mark, K. Aikawa, F. Ferlaino, J. L. Bohn, C. Makrides, A. Petrov, and S. Kotochigova, Nature (London) **507**, 475 (2014).
[13] M. Aßmann, J. Thewes, D. Fröhlich, and M. Bayer, Nat. Mater. **15**, 741 (2016).
[14] W. Zhou, Z. Chen, B. Zhang, C. H. Yu, W. Lu, and S. C. Shen, Phys. Rev. Lett. **105**, 024101 (2010).
[15] J. M. Deutsch, Phys. Rev. A **43**, 2046 (1991).
[16] M. Srednicki, Phys. Rev. E **50**, 888 (1994).
[17] M. Rigol, V. Dunjko, and M. Olshanii, Nature (London) **452**, 854 (2008).
[18] M. Sieber and K. Richter, Phys. Scr. **2001**, 128 (2001).
[19] S. Müller, S. Heusler, P. Braun, F. Haake, and A. Altland, Phys. Rev. Lett. **93**, 014103 (2004).
[20] S. Müller, S. Heusler, P. Braun, F. Haake, and A. Altland, Phys. Rev. E **72**, 046207 (2005).
[21] A. Kitaev, in *A simple model of quantum holography, KITP Strings Seminar and Entanglement 2015 program* (2015), http://online.kitp.ucsb.edu/online/entangled15/.
[22] A. M. García-García and J. J. M. Verbaarschot, Phys. Rev. D **94**, 126010 (2016).
[23] J. S. Cotler, G. Gur-Ari, M. Hanada, J. Polchinski, P. Saad, S. H. Shenker, D. Stanford, A. Streicher, and M. Tezuka, J. High Energy Phys. 05 (2017) 118.
[24] P. Saad, S. H. Shenker, and D. Stanford, arXiv:1806.06840.
[25] A. Chan, A. De Luca, and J. T. Chalker, Phys. Rev. X **8**, 041019 (2018).
[26] P. Kos, M. Ljubotina, and T. c. v. Prosen, Phys. Rev. X **8**, 021062 (2018).
[27] A. Chan, A. De Luca, and J. T. Chalker, Phys. Rev. Lett. **121**, 060601 (2018).
[28] B. Bertini, P. Kos, and T. c. v. Prosen, Phys. Rev. Lett. **121**, 264101 (2018).
[29] D. Basko, I. Aleiner, and B. Altshuler, Ann. Phys. (Amsterdam) **321**, 1126 (2006).
[30] V. Oganesyan and D. A. Huse, Phys. Rev. B **75**, 155111 (2007).
[31] J. Šuntajs, J. Bonča, T. c. v. Prosen, and L. Vidmar, Phys. Rev. E **102**, 062144 (2020).
[32] A. Prakash, J. H. Pixley, and M. Kulkarni, Phys. Rev. Res. **3**, L012019 (2021).
[33] J. Cotler, N. Hunter-Jones, J. Liu, and B. Yoshida, J. High Energy Phys. 11 (2017) 048.
[34] A. del Campo, J. Molina-Vilaplana, and J. Sonner, Phys. Rev. D **95**, 126008 (2017).
[35] A. Altland and D. Bagrets, Nucl. Phys. **B930**, 45 (2018).
[36] J. Liu, Phys. Rev. D **98**, 086026 (2018).
[37] Y. Liao, A. Vikram, and V. Galitski, Phys. Rev. Lett. **125**, 250601 (2020).
[38] A. Chan, A. De Luca, and J. T. Chalker, Phys. Rev. Res. **3**, 023118 (2021).
[39] D. Roy and T. c. v. Prosen, Phys. Rev. E **102**, 060202(R) (2020).
[40] J. Šuntajs, T. Prosen, and L. Vidmar, Ann. Phys. (Amsterdam) **435**, 168469 (2021), special issue on Philip W. Anderson.
[41] M. Winer and B. Swingle, Phys. Rev. X **12**, 021009 (2022).
[42] J. Cornelius, Z. Xu, A. Saxena, A. Chenu, and A. del Campo, Phys. Rev. Lett. **128**, 190402 (2022).
[43] M. Winer, R. Barney, C. L. Baldwin, V. Galitski, and B. Swingle, J. High Energy Phys. 09 (2022) 032.
[44] K. Wittmann W., E. R. Castro, A. Foerster, and L. F. Santos, Phys. Rev. E **105**, 034204 (2022).
[45] L. K. Joshi, A. Elben, A. Vikram, B. Vermersch, V. Galitski, and P. Zoller, Phys. Rev. X **12**, 011018 (2022).
[46] Z. Gong, C. Sünderhauf, N. Schuch, and J. I. Cirac, Phys. Rev. Lett. **124**, 100402 (2020).
[47] S. J. Garratt and J. T. Chalker, Phys. Rev. X **11**, 021051 (2021).
[48] J. Preskill, Quantum **2**, 79 (2018).
[49] E. Altman *et al.*, PRX Quantum **2**, 017003 (2021).
[50] A. Elben, S. T. Flammia, H.-Y. Huang, R. Kueng, J. Preskill, B. Vermersch, and P. Zoller, Nat. Rev. Phys. **5**, 9 (2023).
[51] See Supplemental Material at http://link.aps.org/supplemental/10.1103/PhysRevLett.134.010402 for the architecture and the experimental parameters of the quantum processors, more numerical results, and applied error mitigation techniques.
[52] D. Abanin, J. Bardarson, G. De Tomasi, S. Gopalakrishnan, V. Khemani, S. Parameswaran, F. Pollmann, A. Potter, M. Serbyn, and R. Vasseur, Ann. Phys. (Amsterdam) **427**, 168415 (2021).
[53] The connected SFF is defined as $K_{\mathrm{con}}(t) = K(t) - (1/N^2)\left|\overline{\sum_a e^{iE_a t}}\right|^2$ where the initial nonuniversal dip behavior in $K(t)$ due to inhomogeneities in the density of states is removed.
[54] M. V. Berry, M. Tabor, and J. M. Ziman, Proc. R. Soc. A **356**, 375 (1977).
[55] T. Brydges, A. Elben, P. Jurcevic, B. Vermersch, C. Maier, B. P. Lanyon, P. Zoller, R. Blatt, and C. F. Roos, Science **364**, 260 (2019).
[56] H. Gharibyan, M. Hanada, S. H. Shenker, and M. Tezuka, J. High Energy Phys. 07 (2018) 124.
[57] C. B. Dağ, S. I. Mistakidis, A. Chan, and H. R. Sadeghpour, Commun. Phys. **6**, 136 (2023).
[58] T. Yoshimura, S. J. Garratt, and J. T. Chalker, arXiv:2312.14234.
[59] S. Shivam, A. De Luca, D. A. Huse, and A. Chan, Phys. Rev. Lett. **130**, 140403 (2023).

End Matter

Appendix—For a circular unitary ensemble, the spectral form factor is derived by utilizing the random matrix theory [2] as

$$K_{\mathrm{CUE}}(\tau)=\begin{cases}\frac{\tau}{\tau_{\mathrm{H}}N} & \text{for } 0<\tau\leq\tau_{\mathrm{H}},\\ \frac{1}{N} & \text{for } \tau>\tau_{\mathrm{H}},\end{cases} \tag{A1}$$

whereas for Gaussian orthogonal ensemble, the connected spectral form factor [53] reads

$$K_{\mathrm{GOE}}(t)=\begin{cases}\frac{1}{N}\left[\frac{2t}{t_{\mathrm{H}}}-\frac{t}{t_{\mathrm{H}}}\ln\left(1+\frac{2t}{t_{\mathrm{H}}}\right)\right] & \text{for } t\leq t_{\mathrm{H}},\\ \frac{1}{N}\left[2-\frac{t}{t_{\mathrm{H}}}\ln\left(\frac{2t/t_{\mathrm{H}}+1}{2t/t_{\mathrm{H}}-1}\right)\right] & \text{for } t>t_{\mathrm{H}}.\end{cases} \tag{A2}$$

Recovering the SFF of a quantum many-body system from the experimental data with decoherence is challenging. In this work, we adopt two simple methods to mitigate these errors. First, we apply a formula derived in [45] under the assumption that the decoherence can be approximated by a global depolarization channel (see Supplemental Material for more details). Second, we rescale the experimental data with the ratio between the numerics of the SFF in the presence and absence of decoherence (see Fig. 2). We find that both methods qualitatively recover the ramp-plateau behavior with plateau times that are consistent with our expectations.